Impedance-based Analysis of Harmonic Instabilities in HVDC-Connected Offshore Wind Power Plants

Marc Cheah-Mane[a], Luis Sainz[b], Eduardo Prieto-Araujo[a], Oriol Gomis-Bellmunt[a]

[a]*Centre d'Innovació Tecnològica en Convertidors Estàtics i Accionaments (CITCEA-UPC), ETS d'Enginyeria Industrial de Barcelona, Universitat Politècnica de Catalunya, Av. Diagonal, 647, Pl. 2. 08028 Barcelona, Spain (marc.cheah@upc.edu, eduardo.prieto-araujo@citcea.upc.edu, oriol.gomis@upc.edu)*

[b]*Departament d'Enginyeria Elèctrica, ETS d'Enginyeria Industrial de Barcelona, Universitat Politècnica de Catalunya, Av. Diagonal, 647, Pl. 2. 08028 Barcelona, Spain (sainz@ee.upc.edu)*

Abstract

HVDC-connected Offshore Wind Power Plants (OWPPs) with a large number of power converters are prone to instabilities due to interactions with converter controllers. This paper analyzes harmonic instabilities in OWPPs connected through HVDC due to interactions with the offshore HVDC converter and the wind turbine converters. An impedance-based model is used to represent a detailed OWPP with fully-rated converter based wind turbines, including the offshore HVDC converter, wind turbine converters, submarine cables and transformers of the offshore AC grid. Harmonic stability is evaluated both from the grid connection point of the offshore HVDC converter and the WT grid side converters. As a result, the influence that parameters of converter control systems and the offshore grid configuration have on harmonic resonant frequencies and stability conditions is analyzed in depth through a sensitivity analysis. Active damping implemented as a feed-forward control is coordinated in all converters to mitigate the harmonic instabilities. Examples of harmonic instabilities and active damping application are validated with time domain simulations in PSCAD/EMTDC.

Keywords: Harmonic stability, impedance-based representation, offshore wind power plant, active damping

1. Introduction

Offshore Wind Power Plants (OWPPs) connected through HVDC are isolated systems with high penetration of power electronics that are prone to instability due to electrical resonance interactions. Resonance instabilities have been reported in BorWin1 [1], which was the first HVDC-connected OWPP, and have been highlighted by CIGRE Working Groups, system operators and manufacturers as a potential problem to address [1, 2, 3, 4]. In isolated offshore AC grids, the equivalent capacitance of submarine cables and the equivalent inductance of transformers originate electrical resonances in

Email address: marc.cheah@upc.edu . Tel. +34 934010937 (Marc Cheah-Mane)

the harmonic frequency range [1, 2, 3]. These resonances are poorly damped due to a lack of load and high penetration of power electronics in the offshore AC grid [3]. The controls of the offshore HVDC converter and the Wind Turbine (WT) converters can further reduce the damping at harmonic resonances until instability.

Frequency domain methods are used to identify resonant frequencies and analyze stability without a detailed information for all elements compared to the classical eigenvalue analysis. Methods based on an impedance characterization of the system represent the frequency response of the grid and converters from their connection point. The impedance frequency response can be obtained through a frequency scan from black-box simulation models or real measurements [5, 6]. This represents an advantage for manufacturers and system operators, who can provide the impedance frequency response of converters or the grid without compromising their intellectual property [1].

Resonance stability in HVDC-connected OWPPs has been analyzed in the literature [7, 8, 9, 10, 11, 12, 13]. Oscillation modes of all the frequency spectrum are identified in [11, 13] using an eigenvalue analysis and considering different operational conditions and control parameters. Also, subsynchronous resonances have been analyzed in depth using impedance-based models [8, 9, 10]. However, harmonic resonances have not been analyzed in detail considering the effect of configuration and control parameters. In addition, most of the references use aggregated models to represent wind farms [8, 9, 10, 12], which is useful to validate the results in an experimental test-rig, as presented in [12], but can result in misleading conclusions as reported in [13].

Instabilities caused by resonance interaction can be mitigated with active damping introduced by additional converter controllers: modifying the current control design [14, 12], as a feed-forward control [9] and with band-pass filters that attenuate specific resonant frequencies [14, 15]. Active damping can be used as a virtual impedance to ensure that the converter is passive at the resonant frequencies [16]. In particular, the application of active damping to shape the equivalent impedance of an offshore HVDC converter was presented in [9]. To the best knowledge of the authors, a coordinated strategy of all converters connected to an OWPP to damp different oscillation modes have not been reported in the literature and must be studied in detail.

This paper analyzes harmonic interactions in a HVDC-connected OWPP with fully-rated converter based WTs, which represents an isolated ac system only with converters. Such interactions are identified as oscillations at harmonic resonance frequencies caused by the offshore HVDC converter, WT converters and offshore AC grid. The stability of these oscillation modes is determined by the total damping contribution from the converters and the offshore grid at the resonance frequencies. Har-

monic interactions between the offshore HVDC converter and the offshore grid were reported in [7] considering only the effect of the HVDC converter control, the export cable length and the number of connected WTs. This paper extends the work in [7] by analyzing interactions between the WTs and the offshore grid and by considering the influence of all parameters of the converter control systems and the offshore grid configuration. The contributions are summarized as follows:

- The harmonic interactions are analyzed in a full model of a HVDC-connected OWPP with a detailed representation of the offshore AC grid, *i.e* including all string cables, collector transformers and WT grid side converters.
- The main harmonic resonances are identified with an approximated frequency range, which is defined through a sensitivity analysis of controllers and configuration parameters. Also, simplified expressions of the resonance frequencies are obtained considering the parameters with a significant effect.
- Recommendations about the elements that contribute to the interactions are presented according to the effect of controls implemented in the converters and the offshore grid configuration.
- A coordinated active damping strategy in the offshore HVDC converter and WT converters is presented to mitigate harmonic instabilities.

A detailed OWPP is modeled including all converters, cables and transformers. An impedance-based representation is used to identify resonances and assess stability from the grid connection point of the converters. In particular, the positive-net-damping criterion in [7, 17] is used to evaluate stability conditions. In addition, harmonic instabilities and active damping application are validated in time-domain simulations using PSCAD/EMTDC.

2. Impedance-based model of an HVDC-connected OWPP

Fig. 1a shows a general scheme of an OWPP connected throught HVDC. Fully-rated converter based WTs are considered in this configuration, since this is the preferred topology for high rated power offshore WTs to increase reliability. WTs are connected to string AC cables that transfer the power generation to the offshore collector substation of a wind farm, where transformers are used to step-up from medium to high voltage. Export AC cables from each collector substation are connected to an offshore HVDC converter, which is based on a Modular Multilevel Converter (MMC). This converter operates in grid-forming mode and delivers the wind power generation to the onshore AC grid through a DC transmission link. An onshore HVDC converter regulates the voltage of the DC

transmission link. It is supposed that the offshore AC grid is decoupled from the onshore AC grid dynamics through the DC link [11]. Therefore, the onshore AC grid, onshore HVDC converter and DC transmission system are not represented in this study.

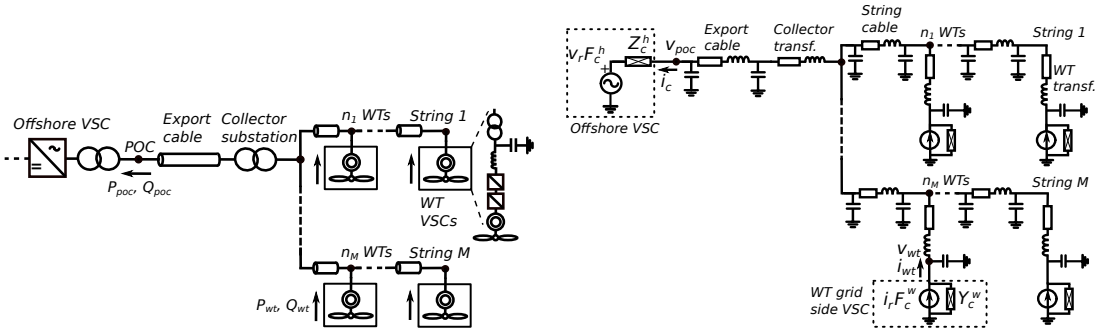

(a) General scheme. (b) Impedance-based model.

Figure 1: Offshore wind power plant connected to an offshore HVDC converter: (a) general scheme and (b) impedance-based model.

An impedance-based model of an HVDC-connected OWPP is used to identify harmonic resonances and analyze stability. Fig. 1b shows the representation of the offshore AC grid, offshore HVDC converter and WT converters with equivalent impedances. It is observed that compared to [9, 10] the full offshore AC grid system is included in the impedance-based model instead of an aggregated representation. The equivalent models are expressed in a stationary $\alpha\beta$ frame and the Laplace s domain. Complex space vectors are used due to the symmetry of the cable, transformers and Voltage Source Converter (VSC) models [18]. Voltages and currents are denoted in boldface letters as $\mathbf{v^s} = v_\alpha + jv_\beta$ and $\mathbf{i^s} = i_\alpha + ji_\beta$.

2.1. Cable and transformer models

The AC cables are modeled as single π-sections with lumped parameters, which is sufficient since the cables are short, and the transformers are modeled as RL equivalents. These cable and transformer models are accurate enough to characterize harmonic resonances and determine stability conditions.

2.2. VSC models

VSCs are represented with the inner control loops, as shown in Fig. 2, which are sufficient to analyze interactions with resonances in the harmonic frequency range. Outer control loops, *e.g.* PLL, DC voltage control or power control, are not included in the VSC models since their dynamic response is slow and they interact with resonances near the synchronous frequency or below (subsynchronous resonances) [19, 20]. In case of an MMC, the internal dynamics of the submodules are not considered since their controllers, *e.g.* circulating current control or energy control, also have a slow dynamic response with interactions below the synchronous frequency [10, 20]

The VSCs are modeled as Thevenin or Norton equivalents according to the converter operation. This equivalent model represents the frequency response of the converters as an impedance or admittance [21]. The VSC models are initially obtained in a synchronous dq frame, where voltages and currents are denoted in boldface letters as $\mathbf{v} = v_d + jv_q$ and $\mathbf{i} = i_d + ji_q$. These models are expressed in $\alpha\beta$ frame employing a reference frame transformation from dq to $\alpha\beta$ frame that is represented as the rotation $s \rightarrow s - j\omega_1$ [22, 23].

The offshore HVDC converter controls the AC voltage of the offshore grid based on the control structure in Fig. 2a. PLL is not required, because the converter is forming the AC grid voltage and the angle is obtained from an oscillator. As a result, this converter is represented in dq frame by a Thévenin equivalent:

$$\mathbf{v_{poc}} = \mathbf{v_r} \cdot F_c^{h,dq} - \mathbf{i_c} \cdot Z_c^{h,dq} \tag{1}$$

where $\mathbf{v_{poc}}$ is the voltage measured at the Point of Connection (POC), $\mathbf{v_r}$ is the control reference voltage at the POC, $F_c^{h,dq}$ is the offshore HVDC converter closed-loop transfer function, $\mathbf{i_c}$ is the current from the offshore HVDC converter and $Z_c^{h,dq}$ is the VSC impedance. Terms $F_c^{h,dq}$ and $Z_c^{h,dq}$ can be expressed as in [7], but adding the VSC delay:

$$F_c^{h,dq} = \frac{D^h F_{\mathrm{PI},v}}{1 + D^h F_{\mathrm{PI},v}};\ Z_c^{h,dq} = \frac{R_f^h + sL_f^h + j\omega_1 L_f^h}{1 + D^h F_{PI,v}} \tag{2}$$

$$F_{\mathrm{PI},v} = k_{p,v} + \frac{k_{i,v}}{s};\ D^h = e^{-sT_d^h} \tag{3}$$

where $F_{\mathrm{PI},v}$ is the PI controller for the voltage control loop, D^h and T_d^h are the offshore VSC delay and its corresponding time delay, L_f^h and R_f^h are the coupling inductance and its equivalent resistance and $\omega_1 = 2\pi f_1$ rad/s ($f_1 = 50$ Hz). The time delay of a VSC, T_d, can be expressed as $T_d = q_d T_s$ [19], where T_s is the sampling time and q_d is a factor that depends on the sampling technique and computation time. Assuming a sampling technique based on a double-update PWM, q_d is equal to 1.5 [19]. Fig. 1b shows the Norton equivalent representation of the WT converters (marked with a dashed black box), where F_c^h and Z_c^h are expressed in $\alpha\beta$ frame by introducing $s \rightarrow s - j\omega_1$

The WTs are equipped with a back-to-back converter, but only the grid side VSC is modeled because the generator side VSC is supposed to be decoupled from the AC side dynamics by the DC link between the VSCs. The WT grid side converters control DC voltage and reactive power, but only the inner current loop is represented for harmonic interaction analysis based on the control structure in Fig. 2b. As a result, these converters are represented in dq frame by a Norton equivalent:

$$\mathbf{i_{wt}} = \mathbf{i_r} \cdot F_c^{w,dq} - \mathbf{v_{wt}} \cdot Y_c^{w,dq} \tag{4}$$

where $\mathbf{i_{wt}}$ is the current from the WT VSC, $\mathbf{i_r}$ is the control reference current, $F_c^{w,dq}$ is the WT VSC closed-loop transfer function, $\mathbf{v_{wt}}$ is the voltage after the coupling filter and Y_c^w is the VSC admittance. Terms $F_c^{w,dq}$ and $Y_c^{w,dq}$ are expressed as in [17]:

$$F_c^{w,dq} = \frac{D^w F_{\mathrm{PI},c}}{R_f^w + sL_f^w + j\omega_1 L_f^w + D^w(F_{\mathrm{PI},c} - j\omega_1 L_f^w)};\ Y_c^{w,dq} = \frac{1 - D^w H_v}{R_f^w + sL_f^w + j\omega_1 L_f^w + D^w(F_{\mathrm{PI},c} - j\omega_1 L_f^w)} \tag{5}$$

$$F_{\mathrm{PI},c} = k_{p,c} + \frac{k_{i,c}}{s};\ H_v = \frac{\alpha_f}{s + \alpha_f};\ D^w = e^{-sT_d^w} \tag{6}$$

where $F_{\mathrm{PI},c}$ is the PI controller of the current loop, L_f^w and R_f^w are the coupling inductance and its equivalent resistance, H_v and α_f are the low pass filter of the voltage feed-forward term and its bandwidth and D^h and T_d^h are the WT VSC delay and its corresponding time delay. The PI design is based on [24], with proportional and integral gains given as $k_{p,c} = \alpha_c L_f^w$ and $k_{i,c} = \alpha_c R_f^w$, and the bandwidth of the current control by α_c. Fig. 1b shows the Thevenin equivalent representation of the offshore HVDC converter (marked with a dashed black box), where F_c^w and, Y_c^w are expressed in $\alpha\beta$ frame by introducing $s \rightarrow s - j\omega_1$.

More details about the Thévenin and Norton equivalent VSC models are found in [7, 17]. Also, the validation of the impedance-based models is detailed in Appendix B.

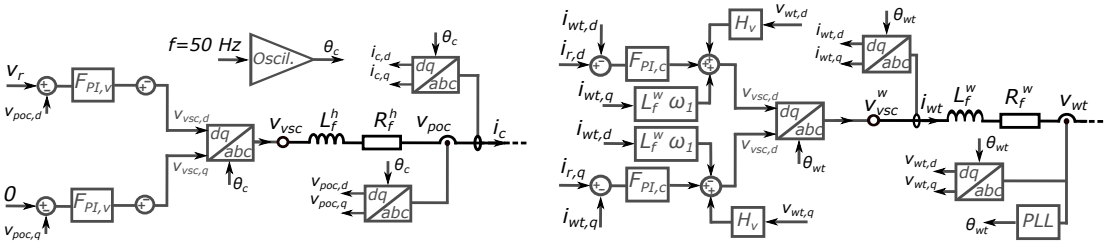

(a) Offshore HVDC converter (b) WT grid side converter

Figure 2: VSC control structures.

The frequency response of Z_c^h and Y_c^w are expressed as:

$$Z_c^h(\omega) = R_c^h(\omega) + jX_c^h(\omega);\ \ Y_c^w(\omega) = G_c^w(\omega) + jB_c^w(\omega) \tag{7}$$

where ω is the frequency in rad/s. The real and imaginary part of Z_c^h and Y_c^w are approximated if $k_{i,v}/\omega \approx 0$, $k_{i,c}/\omega \approx 0$, $R_f^h << L_f^h\omega$ and $\omega >> \omega_1, \alpha_c$:

$$R_{c,ap}^h(\omega) = \frac{-\omega L_f^h k_{p,v} sin(T_d^h\omega)}{k_{p,v}^2 + 1};\ X_{c,ap}^h(\omega) = \frac{\omega L_f^h}{k_{p,v}^2 + 1} = \omega L_c^h \tag{8}$$

$$G_{c,ap}^w(\omega) = \frac{\alpha_c cos(T_d^w\omega) - \omega_0 sin(T_d^w\omega)}{\omega^2 L_f^w};\ B_{c,ap}^w(\omega) = -1/(\omega L_f^w) \tag{9}$$

It is observed that $X_{c,ap}^w$ and $B_{c,ap}^w$ are represented as inductances and $Z_{c,ap}^h$ is non-passive for low

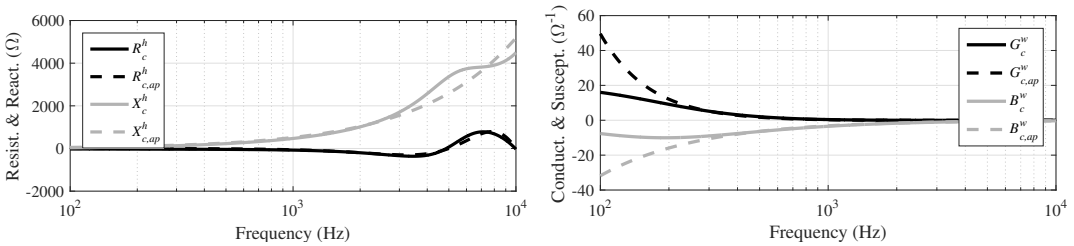

(a) Offshore HVDC converter (b) WT grid side converter

Figure 3: Comparison of approximated and full expressions of R_c^h, X_c^h, G_c^w and B_c^w for harmonic frequencies.

frequencies ($R_{c,ap}^h$ is negative up to 5 kHz). Approximations of Z_c^h are valid for frequencies up to 3 kHz, whereas approximations of Y_c^w are valid for frequencies higher than 300 Hz, as shown in Fig. 3. These approximations will be used to obtain expressions of resonant frequencies in Section 3. However, they might not be accurate to evaluate stability, because the effect of some control parameters is neglected.

3. Identification of harmonic resonances

Harmonic resonances are identified from the grid connection point of the offshore HVDC converter and WT grid side converters. Each resonance will be characterized with a specific frequency, considering the case study described in Appendix A, and a frequency range determined from a sensitivity analysis. Resonant frequencies are affected by the offshore grid topology and the design parameters chosen by the manufacturers. The intersections between magnitudes of the converter impedance and the equivalent grid impedance observed from the converter approximately determine the resonant frequencies. Therefore, in this Section the frequency response of the magnitudes is enough to identify resonances.

3.1. Resonances from the Offshore HVDC converter

The equivalent grid impedance from the offshore HVDC converter, Z_g^h, is obtained as series-parallel combinations of the impedances of cables, transformers and WT converters, as shown in Fig. 4a. Resonances from the offshore HVDC converter are identified in the frequency response when $Z_c^h + Z_g^h$ has a dip or peak (series or parallel resonance). This is approximately equal to frequencies where $|Z_c^h| = |Z_g^h|$ when resistive components are negligible compared to reactive components. Series resonances can cause instability in the offshore VSC due to its operation as AC voltage control. Fig. 4b shows the frequency response of the offshore VSC impedance, Z_c^h, the equivalent impedance of the grid from this converter, Z_g^h, and $Z_c^h + Z_g^h$. In this case, a series resonance is identified at $f_{res}^h = 403.2$ Hz.

The effect that control parameters and OWPP configuration have on the resonant frequency is analyzed in Fig. 5, where the variation of these parameters is from 1/5 to 5 times the initial values

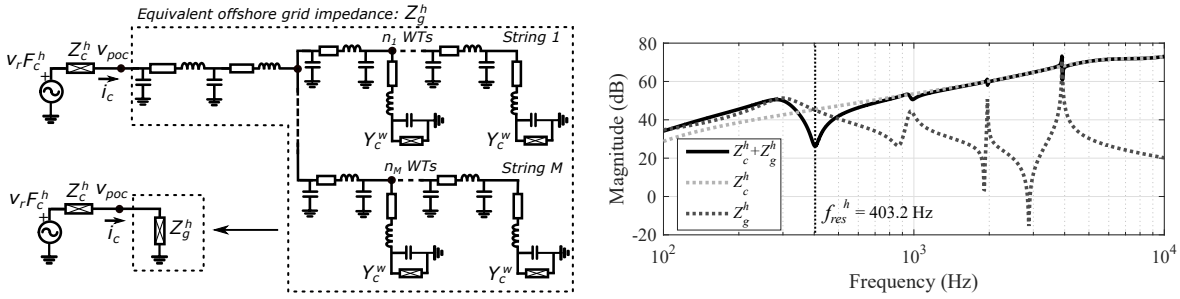

(a) Electrical scheme (b) Frequency response of $Z_c^h + Z_g^h$, Z_c^h and Z_g^h

Figure 4: Representation of equivalent grid impedance from the offshore HVDC converter

defined in Appendix A. Transformers and converter reactors are not considered, because their values are supposed to be fixed during the converter and offshore AC grid design.

Control parameters of the offshore HVDC converter and the WT converters ($k_{p,v}$ and α_c) cause significant variations (*i.e.* more than 5 %), as shown in Fig. 5a. It is observed that high values of α_c reduce the resonant frequency down to 240 Hz. However, high values of α_c might not be possible since they are limited by the switching frequency, ω_{sw}, of the WT converters ($\alpha_c \leq 0.2\omega_{sw}$ [24]).

The export cable length, $l_{exp,cab}$, has the highest effect on the resonant frequency with a maximum variation of 200 Hz (50 %). Also, the equivalent capacitor of the WT high frequency filter, C_f^w, and parameters of the offshore grid configuration (total string cable length, $l_{str,cab}$, and number of strings) cause variations up to 80 Hz (20 %), as shown in Figs. 5b-5c. In light of these results, the series resonance from the offshore HVDC converter is in the range of 200 $\sim$ 600 Hz.

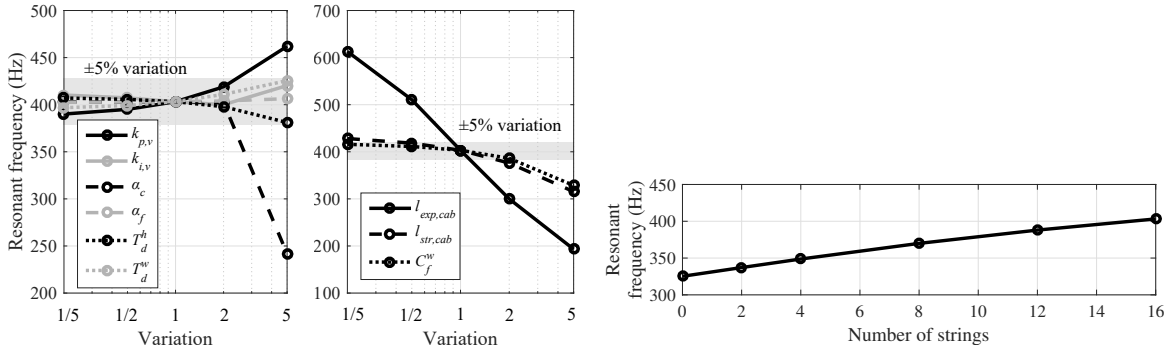

(a) Control parameters (b) Config. parameters (c) Number of strings of offshore wind farm

Figure 5: Sensitivity of resonant frequency from offshore HVDC converter with variation of (a) control parameters, (b) configuration parameters and (c) number of strings of offshore wind farm.

The equivalent offshore grid from the offshore HVDC converter can be simplified as shown in Fig. 6a, where the parameters that have a small contribution to the series resonant frequency have been neglected. String cables are aggregated with the following parameters:

- $C_{str,ag}$ is the aggregated capacitance of the string cables according to the configuration described

in Appendix A and is expressed as $C_{str,ag} = N_{str}(C_{str,1}l_{str,1} + 4C_{str,2}l_{str,2})$, where $C_{str,1}$ and $C_{str,2}$ are string cable capacitances per kilometer, $l_{str,1}$ and $l_{str,2}$ are string cable lengths and N_{str} is the number of strings.

- $C^w_{f,ag}$ is the aggregated capacitance of the WT high frequency filters and is expressed as $C^w_{f,ag} = 5N_{str}C^w_f$.
- $Y^w_{c,ag}$ is the aggregated admittance of the WT grid side converters and is expressed as $Y^w_{c,ag} = 5N_{str}Y^w_c$.

The inductive and resistive components of the export cable are small enough to be combined with the RL equivalent of the offshore HVDC transformer. Also, the inductance and resistance of the string cables and the RL equivalent of the WT transformers are not represented because they are small and do not affect the series resonant frequency. The simplified equivalent grid impedance is a good approximation of Z^h_g for harmonic frequencies up to 900 Hz, as show in Fig. 6b, which agrees with the frequency range for series resonances (200 $\sim$ 600 Hz). Assuming that $Z^h_c \approx R^h_{c,ap} + j\omega L^h_c$ from (8) and $Y^w_c \approx G^w_{c,ap} - j/(\omega L^w_f)$ from (9), the series resonant frequency is calculated as:

$$\begin{cases} f^h_{res,ap} \approx \dfrac{1}{2\pi}\sqrt{\dfrac{b-\sqrt{b^2-4ad}}{2a}} \\ a = C_{ec}L^w_{c,ag}L^{cs}_{tr}L^h_c(C^w_{f,ag} + C_{str,ag}) \\ b = C_{ec}L^h_c(L^w_{c,ag} + L^{cs}_{tr}) + L^w_{c,ag}(C^w_{f,ag} + C_{str,ag})(L^h_c + L^{cs}_{tr}) \\ d = L^h_c + L^w_{c,ag} + L^{cs}_{tr} \end{cases} \tag{10}$$

where $L^w_{c,ag} = L^h_c/(5N_{str})$.

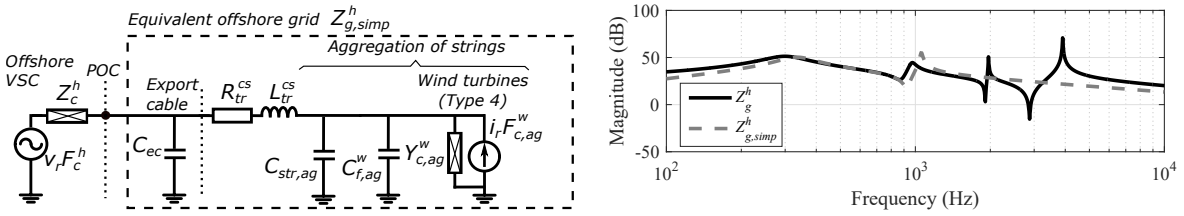

(a) Electrical scheme

(b) Frequency response of Z^h_g and $Z^h_{g,sim}$.

Figure 6: Representation of equivalent grid impedance from the offshore HVDC converter.

3.2. Resonances from Wind Turbine converters

Resonances are analyzed from a WT located at the end of a string cable. The equivalent grid admittance from this WT is obtained as a series-parallel combination of the impedances of cables, transformers, the offshore HVDC converter and other WT converters, as shown in Fig. 7a. Parallel resonances can cause instability in WT grid side converters due to their operation as AC current

control. Fig. 7b shows the frequency response of the WT converter impedance, $Z_c^w = 1/Y_c^w$, the equivalent grid impedance from this converter, $Z_g^w = 1/Y_g^w$, and $1/(Y_c^w + Y_g^w)$. In this case, a main parallel resonance is identified at $f_{res,1}^w = 1288$ Hz.

A second parallel resonance ($f_{res,2}^w = 1172$ Hz) arises close to the main resonance due to interaction with multiple resonances in Z_g^w. Collector grids with long string cables are prone to generate additional parallel resonances around the main resonance, as shown in Fig. 8, where the frequency response of $1/(Y_c^w + Y_g^w)$ is obtained for different cable lengths.

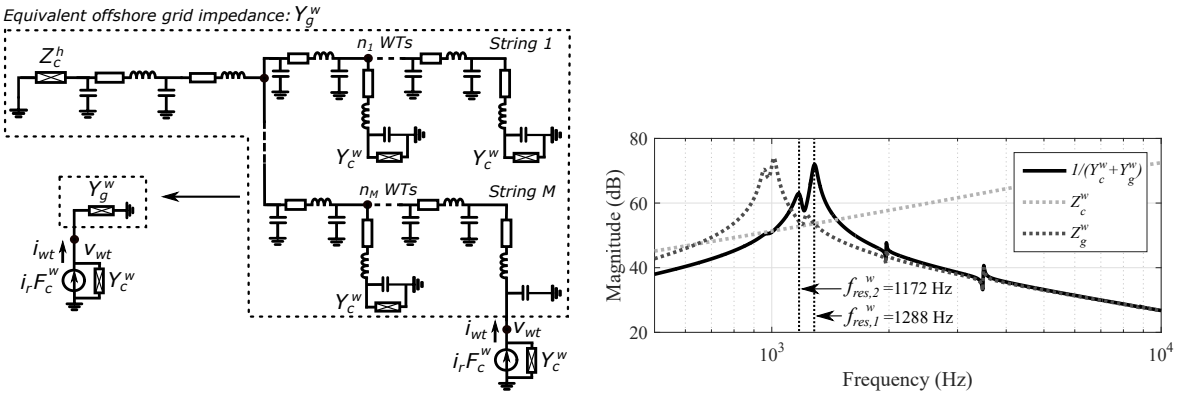

(a) Electrical scheme

(b) Frequency response of $1/(Y_c^w + Y_g^w)$, Z_c^w and Z_g^w.

Figure 7: Representation of equivalent grid impedance from a WT located at the end of a string cable.

The effect that control parameters and OWPP configuration have on the main resonant frequency is analyzed in Fig. 9. It is observed that only control and configuration parameters related to WTs (α_c and C_f^w) cause a significant variation up to 1200 Hz (90 %) for low values of C_f^w. In view of these results, the main parallel resonance is approximately independent of offshore grid configuration and control of other VSCs. Also, parallel resonances from the WT converter are in the range of $500 \sim 2500$ Hz, but if C_f^w variation is not considered the frequency range is narrowed down to $1200 \sim 1400$ Hz.

A simplified equivalent impedance of the offshore grid, $Z_{g,simp}^w$, is defined by the WT transformer, Z_{tr}^w, and the WT high frequency filter, C_f^w, as shown in Fig. 10a. This simplified grid impedance is a good representation of Z_g^w for harmonic frequencies, except for the resonances caused by the string cables, as shown in Fig. 10b. Assuming that $Y_c^w \approx G_{c,a}^w - j/(\omega L_f^w)$ from (9) and $Z_{g,simp}^w \approx Z_g^w$, the main resonant frequency is approximated from a LCL circuit as:

$$f_{res,ap}^w \approx \frac{1}{2\pi}\sqrt{\frac{L_f^w + L_{tr}^w}{C_f^w L_{tr}^w L_f^w}} \tag{11}$$

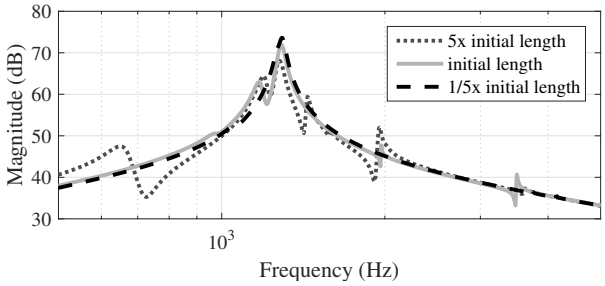

Figure 8: Frequency response of $1/(Y_c^w + Y_g^w)$ with different string cable lengths.

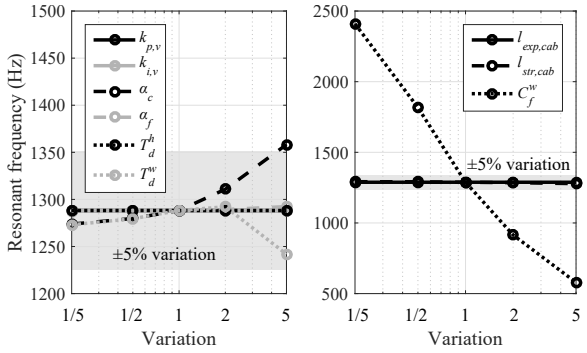

(a) Control parameters (b) Config. parameters

Figure 9: Sensitivity of resonant frequency from WT converters with variation of (a) control parameters and (b) configuration parameters of the offshore wind farm.

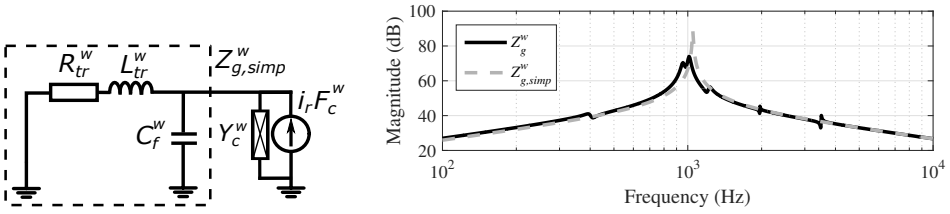

(a) Electrical scheme (b) Frequency response of Z_g^w and $Z_{g,sim}^w$.

Figure 10: Representation of grid side VSC of a WT connected to the simplified equivalent impedance of the offshore grid, $Z_{g,simp}^w$.

4. Resonance stability

Interactions between resonances and VSC control can destabilize the system due to VSC non-passivity. Stability is analyzed from the connection point of each VSC using the frequency response of the converter impedance and the equivalent impedance of the offshore grid observed from the converter.

The positive-net damping criterion defined in [7, 17] is used to evaluate resonance stability at harmonic frequencies. The system is asymptotically stable if the total damping, which is sum of the converter and grid damping, is positive at resonant frequencies. This criterion is equivalent to the impedance-based stability criterion [5], but evaluates the real part of impedances or admittances (*i.e.* resistance or conductances) instead of the phase margin of the ratio between converter and grid equivalent impedances or admittances.

4.1. Analysis from Offshore HVDC converter

In this case, the positive-net-damping criterion is expressed as a total resistance because the converter is represented with a Thévenin equivalent [7]:

$$R_T^h(\omega_{res}) = R_c^h(\omega_{res}) + R_g^h(\omega_{res}) > 0 \tag{12}$$

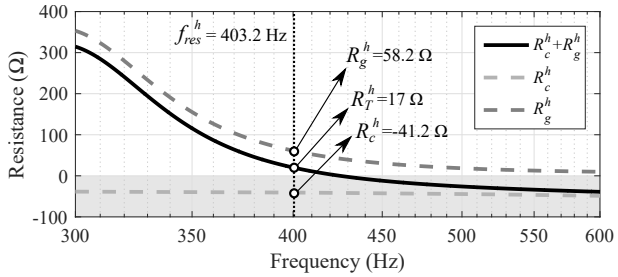

Figure 11: Frequency response of $R_T^h = R_c^h + R_g^h$, R_c^h and R_g^h.

Fig. 11 shows an application example of the positive-net-damping criterion from the offshore HVDC converter. The resistances are evaluated at the series resonant frequency in Fig. 4b. The system is stable since the total resistance, R_T^h, is positive at the resonant frequency, $f_{res}^h = 403.2$ Hz. It can be observed that the HVDC converter is non-passive (*i.e.* $R_c^h < 0$ at the resonant frequency), but the contribution of the offshore grid resistance, R_g^h, ensures the system stability.

The effect that control parameters and OWPP configuration have on stability is analyzed in Fig. 12, where the variation of these parameters is from 1/5 to 5 times the initial values defined in Appendix A. Also, the total resistance R_T^h is evaluated at the resonant frequencies in Fig. 5. The system becomes unstable if the control gains of the offshore HVDC converter, $k_{p,v}$ and $k_{i,v}$, are increased or the control

bandwidth of the WT converter, α_c, is reduced, as shown in Fig. 12a. Also, the increase of T_d^w has a negative impact on stability.

Export cables and C_f^w are passive components with a significant effect on R_T^h. High values of C_f^w shift the resonance to lower frequencies, as shown in Fig. 5b, which increases R_T^h, as shown in Fig. 12b. Long export cables also decrease the resonant frequency, as shown in Fig. 5b, but the frequency response of R_T^h is reduced such that R_T^h at the resonant frequency is lower, as shown in Fig. 12b.

The reduction of connected strings may destabilize the system, as shown in Fig. 12c. In particular, the highest risk of resonance instability is during the energization of the offshore AC grid, *i.e.* when there are not wind turbines connected to the system [7].

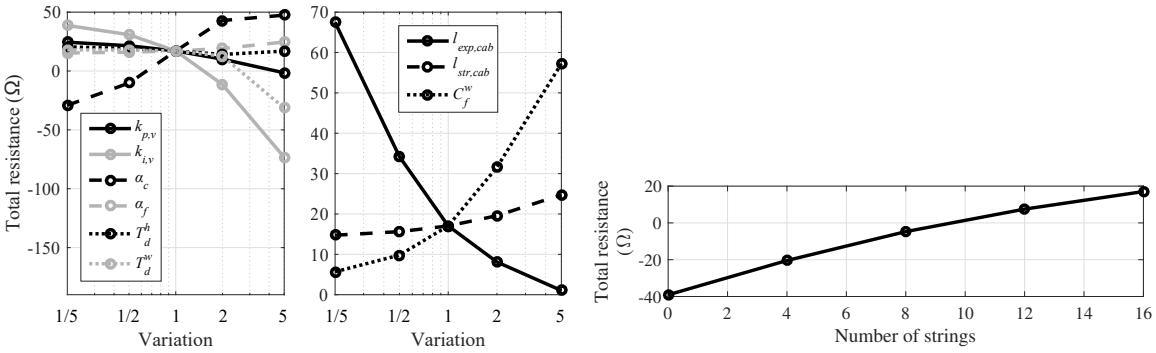

(a) Control parameters (b) Config. parameters (c) Number of strings of offshore wind farm

Figure 12: Sensitivity of $R_T^h(\omega_{res})$ with variation of (a) control parameters, (b) configuration parameters and (c) number of strings of offshore wind farm.

A time domain simulation in PSCAD/EMTDC is used to validate the stability conditions from the positive-net-damping criterion. Fig. 13 shows an example where the interaction of the offshore HVDC converter with the WT converters causes harmonic instability. In this case, α_c is reduced from 1000 to 500 rad/s (1/2 of initial value) at 0.5 s, which leads to instability due to oscillations at 399.5 Hz as determined by the resistance values in Fig. 12. Also, this instability is identified following the Nyquist criterion, since the Nyquist curve of Z_c^h/Z_g^h encircles (-1, 0) in clockwise direction and the open loop system does not have unstable poles when $\alpha_c = 500$ rad/s, as shown in Fig. 13c.

4.2. Analysis from Wind Turbine converters

In this case, the positive-net-damping criterion is expressed as a total conductance because the converter is represented as a Norton equivalent [17]:

$$G_T^w(\omega_{res}) = G_c^w(\omega_{res}) + G_g^w(\omega_{res}) > 0 \tag{13}$$

Fig. 14 shows and application example of the positive-net-damping criterion from the WT located at the end of a string cable. The conductances are evaluated at the two parallel resonant frequencies

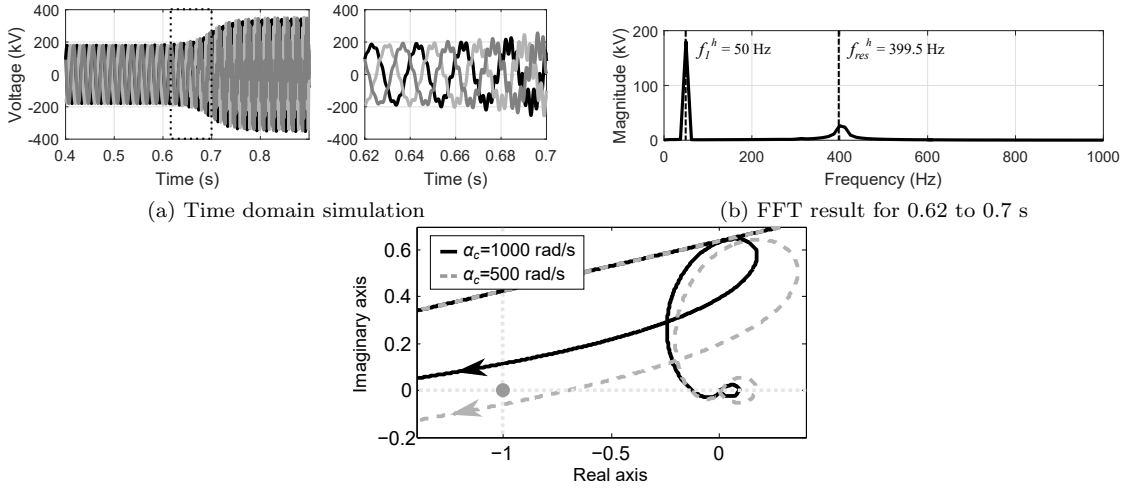

(a) Time domain simulation

(b) FFT result for 0.62 to 0.7 s

(c) Nyquist plot of Z_c^h/Z_g^h (positive frequencies)

Figure 13: Series resonance instability due to reduction of α_c from 1000 to 500 rad/s at 0.5 s.

in Fig. 7b. It is observed that the system is stable since the total conductance, G_T^w, is positive at the resonant frequencies, $f_{res,1}^w$ and $f_{res,2}^w$.

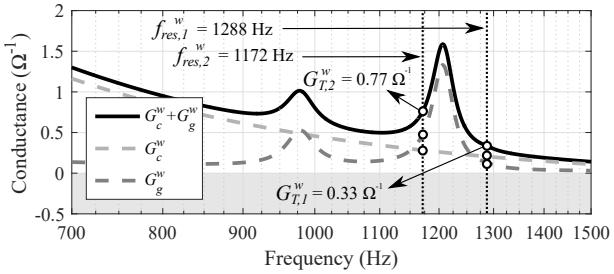

Figure 14: Frequency response of $G_T^w = G_c^w + G_g^w$, G_c^w and G_g^w.

The effect that control parameters and OWPP configuration have on the stability is analyzed in Fig. 15. The total damping is evaluated at the main resonant frequency, $f_{res,1}^w$, according to the values in Fig. 9. Only control and configuration parameters related to the WTs (α_c, T_d^w and C_f^w) cause a significant variation on the damping. Therefore, the stability of WT VSCs can be analyzed independently of the offshore grid configuration and control of other VSCs employing the simplified circuit in Fig. 10a.

A time domain simulation in PSCAD/EMTDC is used to validate the stability conditions from the positive-net-damping criterion. Fig. 16 shows an example, where T_d^w is increased from 0.1 to 0.3 ms (3 times the initial value) at 0.5 s. It is observed that the system is unstable due to oscillations at 1284 Hz as determined by the conductance values in Fig. 15. Also, this instability is identified following the Nyquist criterion, since the Nyquist curve of Y_c^w/Y_g^w encircles (-1, 0) in clockwise direction and

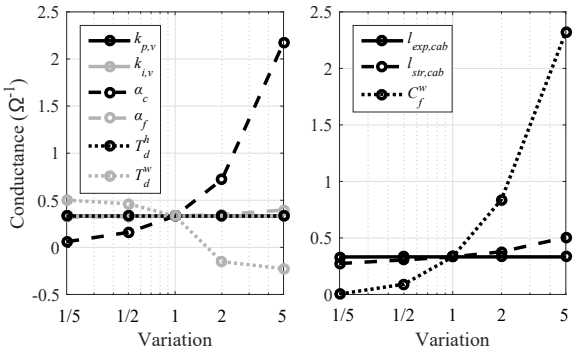

(a) Control parameters (b) Config. parameters

Figure 15: Sensitivity of $G_T^w(\omega_{res,1})$ with variation of (a) control parameters and (b) configuration parameters of the offshore wind farm.

the open loop system does not have unstable poles when $T_d^w = 0.3$ ms, as shown in Fig. 16c.

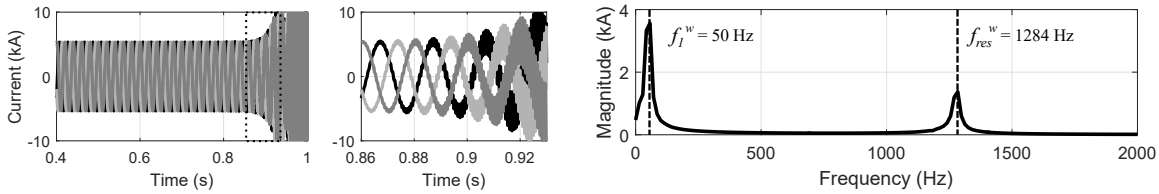

(a) Time domain simulation (b) FFT result for 0.86 to 0.93 s

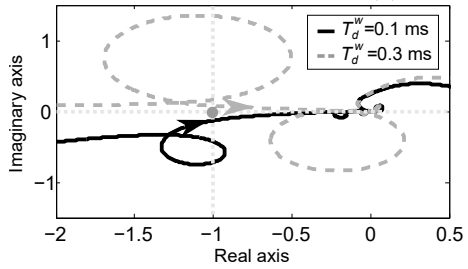

(c) Nyquist plot of Y_c^w/Y_g^w (positive frequencies)

Figure 16: Parallel resonance instability due to increase of T_d^w from 0.1 to 0.3 ms at 0.5 s.

5. Active damping coordination

Resonance instability is solved by introducing active damping as a feed-forward control that increases the real part of the converter impedance or admittance. It should be mentioned that the coordinated strategy presented in this Section is more convenient for an impedance-based representation of the system where the equivalent converter and grid impedances are obtained through a frequency scan from real measurements or black-box simulation models. The active damping control parameters are selected based on the modification of impedance frequency response.

Active damping must be coordinated in all converters connected to the offshore AC grid and should cover all possible resonance frequency variations due operational states or grid configuration. Series and parallel resonances can be approximately divided in two different frequency ranges, as concluded in

Section 3. Therefore, active damping can be limited to the frequency range of each resonance type by using high pass filters with an adequate cutoff frequency. Fig. 17 shows the feed-forward components of the control implemented in the converters, R_a^h and G_a^w, which are expressed as:

$$R_a^h = R_a H_f^h = \frac{R_a s}{s+\omega_n^h};\; G_a^w = G_a H_f^w = \frac{G_a s}{s+\omega_n^w} \tag{14}$$

where R_a and G_a are the feed-forward gains, H_f^h and H_f^w are the high pass filters and ω_n^h and ω_n^w are the cutoff frequencies of the filters. The impedance of the offshore HVDC converter, $Z_{c,a}^{h,dq}$, and the admittance of the WT grid side converters, $Y_{c,a}^{w,dq}$, including active damping are modified as:

$$Z_{c,a}^{h,dq} = \frac{R_f^h + sL_f^h + j\omega_1 L_f^h + D^h R_a^h}{1 + D^h F_{PI,v}};\;\; Y_{c,a}^{w,dq} = \frac{1 - D^w(H_v + G_a^w)}{R_f^w + sL_f^w + j\omega_1 L_f^w + D^w(F_{\mathrm{PI},c} - j\omega_1 L_f^w)} \tag{15}$$

Fig. 18 shows the effect that the active damping has on the converter impedances for different feed-forward gains and cutoff frequencies. It is observed that $R_{c,a}^h$ and $G_{c,a}^w$ increase at high frequencies according to the cutoff frequencies. Note that $G_{c,a}^w$ is reduced at low frequencies when G_a increases or ω_n^w decreases, which could affect the stability of low frequency resonances.

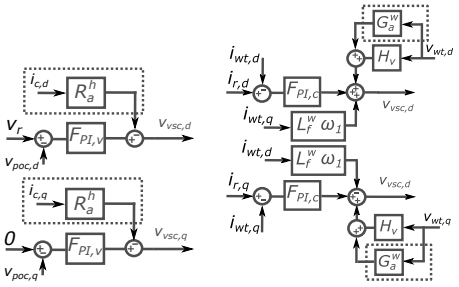

(a) Offshore HVDC converter (b) WT grid side converter

Figure 17: VSC control structures with active damping.

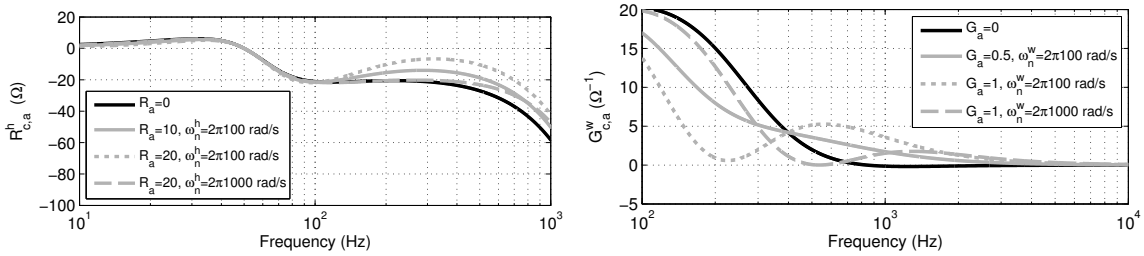

(a) Offshore HVDC converter resistance, $R_{c,a}^h$ (b) WT grid side converter conductance, $G_{c,a}^w$

Figure 18: Variation of converter impedances with active damping.

The stability improvement using active damping is shown for a OWPP with 4 strings (*i.e.* 20 WTs are connected). Results are validated in time domain simulation using PSCAD/EMTDC.

5.1. Application in Offshore HVDC converter

Fig. 19 shows an example of harmonic instability due to the series resonance, where $k_{i,v}$ is modified from 100 to 250 at 0.6 s. The instantaneous voltages at POC in Fig. 19a show an unstable oscillation at 349.6 Hz, which is approximately the value calculated with (10), 344 Hz. When $k_{i,v}$ is 250 the system becomes unstable because R_T^h at the resonant frequency is negative, as observed in Fig. 20a.

Active damping is included in the offshore HVDC converter and the WT grid side converters to increase R_T^h and mitigate the series resonance instability. It is considered $\omega_n^h = 2\pi 100$ rad/s, which is sufficient to cover the frequency range of the series resonance (200 $\sim$ 600 Hz). Active damping in the offshore HVDC converter increases R_c^h at the series resonant frequency to ensure that R_T^h is positive, as shown in Fig. 20a. Active damping in the WT converters reduces R_T^h at low frequencies due to the decrease of G_c^w observed in Fig. 18b. Therefore, series resonance instability is mitigated using active damping in the offshore HVDC converter, which is validated in the time-domain simulation shown in Fig. 20b when R_a= 10. Also, it is concluded that active damping from WT grid side converters is not effective to mitigate the series resonance instability

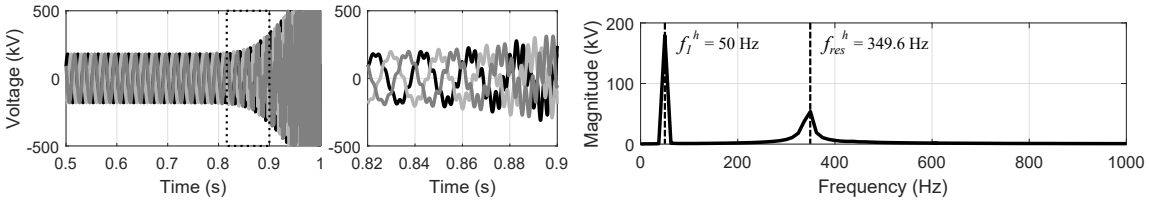

(a) Time-domain simulation results of instantaneous voltages at POC of offshore HVDC converter

(b) FFT result from 0.82 to 0.9 s

Figure 19: Series resonance instability when $k_{i,v}$ is modified from 100 to 250 at 0.6 s and the OWPP have 4 strings

.

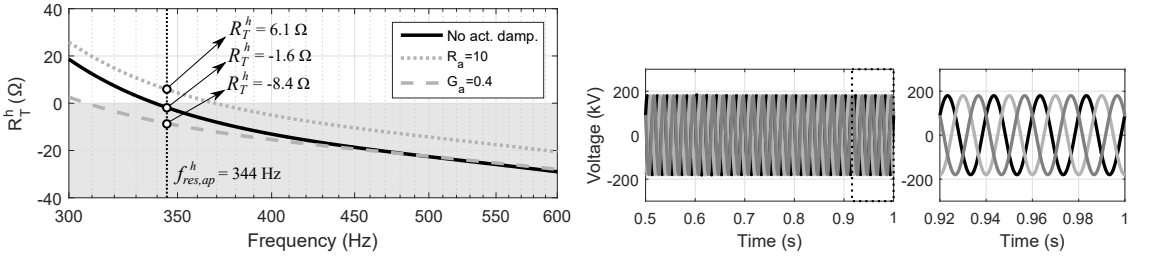

(a) Frequency response of R_T^h with R_a and G_a

(b) Time-domain simulation results of instantaneous voltages at POC of offshore HVDC converter when R_a = 10.

Figure 20: Introduction of active damping to mitigate series resonance instability when $k_{i,v}$ = 250.

5.2. Application in Wind Turbine converters

Fig. 21 shows an example of harmonic instability due to parallel resonance, where T_d^w is modified from 0.1 to 0.3 ms at 0.6 s. The instantaneous currents from the WTs in Fig. 21a show an unstable

oscillation at 1297 Hz, which is approximately the value calculated with (11), 1288 Hz. If T_d^w is 0.3 ms the system becomes unstable because G_T^h at the resonant frequency is negative, as seen in Fig. 22a.

Active damping is included in the offshore HVDC converter and the WT grid side converters to increase G_T^h and mitigate the parallel resonance instability. It is considered $\omega_n^w = 2\pi 500$ rad/s, which covers the frequency range of parallel resonances (500 $\sim$ 2500 Hz). Active damping in the WT converters increases G_T^w, whereas active damping in the offshore HVDC converter does not affect G_T^w, as shown in Fig. 22a. Therefore, parallel resonance instability is mitigated using active damping in the WT converters, which is validated in the time-domain simulation shown in Fig. 22b when G_a= 0.4. Also, it is concluded that active damping from the offshore HVDC converter is not effective to mitigate the series resonance instability.

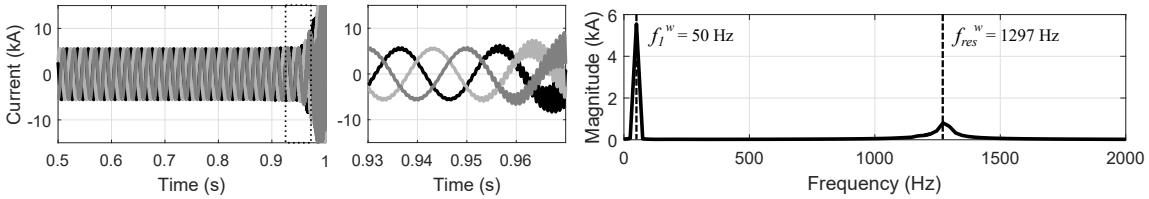

(a) Time-domain simulation results of instantaneous currents from WT grid side converter

(b) FFT result from 0.93 to 0.97 s

Figure 21: Parallel resonance instability when T_d^w is modified from 0.1 to 0.3 ms at 0.6 s and the OWPP have 4 strings.

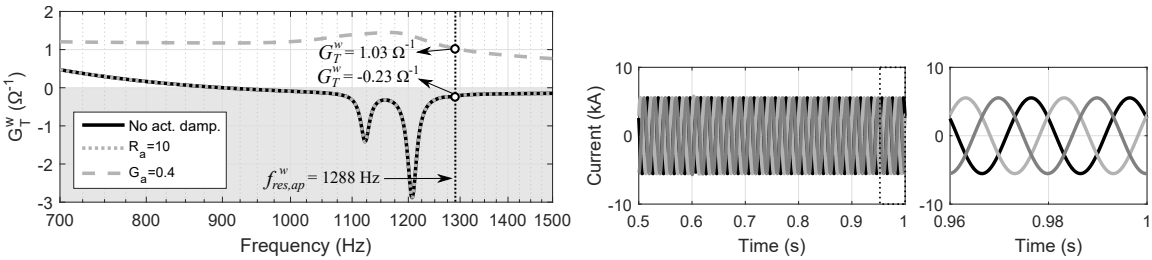

(a) Frequency response of G_T^w with R_a and G_a

(b) Time-domain simulation results of instantaneous currents from WT grid side converter when G_a = 0.4.

Figure 22: Introduction of active damping to mitigate parallel resonance instability when T_d^w = 0.3 ms.

6. Conclusion

Harmonic resonance interactions have been analyzed between the converters and offshore AC grid in a HVDC-connected OWPP. An impedance-based model of the passive components (cables and transformers) and the VSCs (offshore HVDC converter and WT converter) was used to identify the interactions as harmonic resonances with a specific damping, *i.e.* equivalent resistance or conductance. Two main problematic resonances were identified from the grid connection point of the converters:

- Series resonances at 200 $\sim$ 600 Hz that interact with the offshore HVDC converter.

- Parallel resonances at 500 $\sim$ 2500 Hz that interact with grid side WT converters

CIGRE Working Groups, system operators and manufacturers suggest that harmonic frequency oscillations might be originated in a range from a few hundred Hz to above 1 kHz, which agrees with the values found in this paper. Also, approximated expressions of the resonant frequencies, were derived from a sensitivity analysis, which provide a better understanding of the parameters that have a significant effect on the resonant frequencies.

In terms of stability, the following conclusions and recommendations are drawn from the results:

- Harmonic instabilities due to series resonances are affected by the control system of offshore HVDC and WT converters and the offshore grid configuration. Therefore, a complete model of an HVDC-connected OWPP is required to analyze series resonance instabilities.

- Harmonic instabilities due to parallel resonances are mostly affected by the WT configuration and control parameters of the WT grid side converter. Therefore, a simplified model of a single WT is sufficient as a first approach to analyze parallel resonance instabilities.

- Converters are equipped with active damping that only mitigates the harmonic instability interacting with them. Therefore, the offshore HVDC converter will damp series resonance instabilities and the WT grid side converters will damp parallel resonance instabilities. The active damping control is always introduced to cover all possible resonance frequency variations without external information of the system.

Appendix A. OWPP description and control parameters

A 480 MW OWPP is considered in this study. A total number of 80 WTs is distributed in 16 strings of 5 units.

Offshore HVDC VSC: MMC-VSC; rated power, 560 MVA; rated voltage, 320 kV; arm inductance, L_{arm} = 183.7 mH; control gains, $k_{p,v}$= 0.2 and $k_{i,v}$= 500; time delay, T_d^h= 0.1 ms (sampling frequency, f_s = 15 kHz).

Offshore HVDC transformer: 2 units in parallel; rated power, 280 MVA; rated voltages, 350 kV/220 kV; equivalent inductance and resistance at 220 kV, $L_{tr}^h = 99.03$ mH, $R_{tr}^h = 0.86\ \Omega$.

Export cables: 2 cables in parallel; length, $l_{ec} = 10$ km; equivalent lumped parameters per cable at 220 kV, $L_{ec} = 0.4$ mH/km, $R_{ec} = 0.032\ \Omega$/km, $C_{ec} = 0.17\ \mu$F/km.

Collector transformers: 4 units in parallel; rated power of each unit, 140 MVA; rated voltages, 220 kV/33 kV; equivalent inductance and resistance of the transformers at 220 kV, $L_{tr}^{cs} = 20.63$ mH, $R_{tr}^{cs} = 0.22\ \Omega$.

String cables between WTs: cable length; $l_{str,1} = 1.17$ km; equivalent lumped parameters at 33 kV, $L_{str,1}$ = 0.36 mH/km, $R_{str,1} = 0.098\ \Omega$/km, $C_{str,1} = 0.23\ \mu$F/km.

String cables between WT and collector substation: cable length; $l_{str,2} = 4.18$ km; equivalent lumped parameters at 33 kV, $L_{str,2} = 0.31$ mH/km, $R_{str,2} = 0.041\ \Omega$/km, $C_{str,2} = 0.34\ \mu$F/km.

WT transformers: rated power, 6.5 MVA; rated voltages, 33 kV/0.9 kV; equivalent inductance and resistance at 33 kV, $L_{tr}^{w} = 31$ mH, $R_{tr}^{w} = 1.46\ \Omega$.

Grid side WT VSC: 2-level VSC; rated power, 6.5 MVA; rated voltage, 0.9 kV; coupling inductance, $L_{f}^{w} = 50\ \mu$H; coupling resistance, $R_{f}^{w} = 0.02$ mΩ; equivalent capacitance of high frequency filter, $C_{f}^{w} = 1$ mF; low pass filter bandwidth, $\alpha_f = 50$ rad/s; current control bandwidth, $\alpha_c = 1000$ rad/s; time delay, T_{d}^{w}= 0.1 ms (sampling frequency, $f_s = 15$ kHz).

Appendix B. Frequency scan with PSCAD/EMTDC and validation of impedance-based model

Frequency scan of each converter is obtained applying a grid voltage with harmonic magnitudes of 1% the nominal value. Currents and voltages are measured at the converter terminals and an FFT is used to obtain their harmonic components. The frequency response of the impedance is obtained from the harmonic components of the measured currents and voltages, as follows:

$$|Z| = |V|/|I|;\ arg(Z)| = arg(V) - arg(I) \tag{B.1}$$

Figs. B.23 and B.24 show the frequency response of Z_c^h and Y_c^w for harmonic frequencies, where magnitude and phase are compared to frequency scan results using simulation models of the converters in PSCAD/EMTDC. It is observed that there is good agreement between equations and frequency scan results. Also, it should be noted that the validity of the impedance-based based models is limited to harmonic frequencies up to the Nyquist frequency ($f_s/2$), which is equal to 15/2=7.5 kHz for the example shown in Figs. B.23 and B.24. For frequencies above the Nyquist frequency, the delay must be represented with a ZOH model [25], which is not considered in this paper.

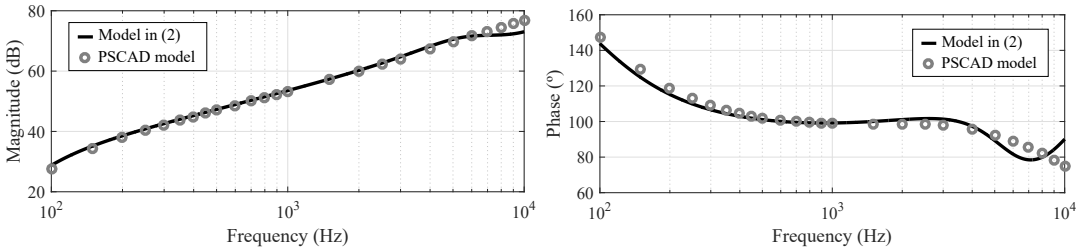

(a) Magnitude of offshore HVDC converter impedance, $|Z_c^h|$

(b) Phase of offshore HVDC converter impedance, $arg(Z_c^h)$

Figure B.23: Frequency response of offshore HVDC converter impedance, Z_c^h. Frequency scan results using simulation model in PSCAD/EMTDC are marked as circles.

In Section 2 the outer loops of the VSC control are simplified for the WT grid side converter. Figs. B.25 and B.26 show a comparison of the impedance frequency response obtained analytically from

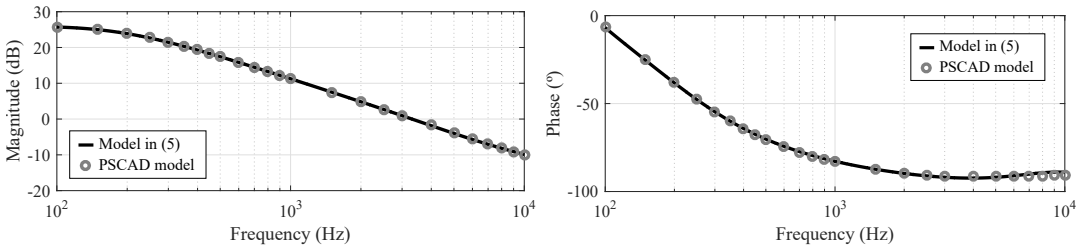

(a) Magnitude of WT grid side converter admittance, $|Y_c^w|$

(b) Phase of WT grid side converter admittance, $arg(Y_c^w)$

Figure B.24: Frequency response of WT grid side converter admittance, Y_c^w. Frequency scan results using simulation model in PSCAD/EMTDC are marked as circles.

equations (2) and (5), and the results obtained from a frequency scan when the PI control gains of the DC voltage control and PLL are increased, *i.e.* the controls are faster.

It is observed that a faster DC voltage shows a significant difference in the frequency response up to 200 Hz, but the PLL does not have a significant effect for frequency higher than 100 Hz.

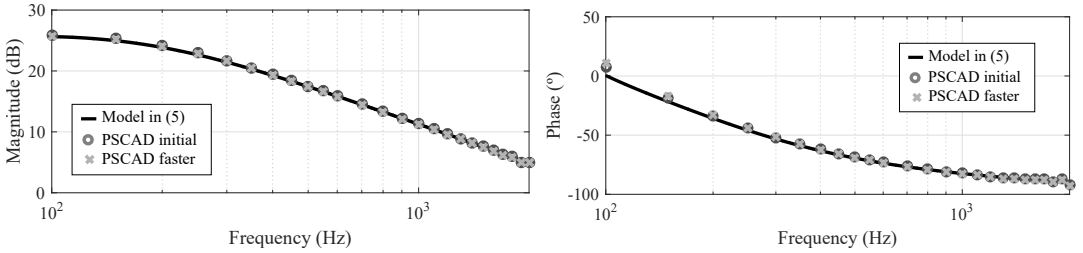

(a) Magnitude of offshore HVDC converter impedance, $|Z_c^h|$

(b) Phase of offshore HVDC converter impedance, $arg(Z_c^h)$

Figure B.25: Comparison of frequency response of WT grid side converter admittance when PLL control gains are 10 times higher

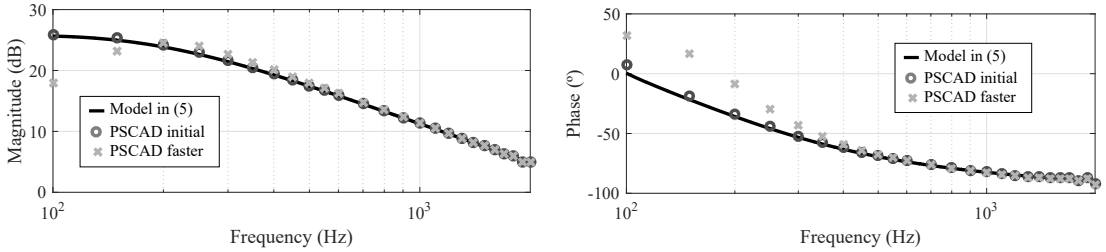

(a) Magnitude of WT grid side converter admittance, $|Y_c^w|$

(b) Phase of WT grid side converter admittance, $arg(Y_c^w)$

Figure B.26: Comparison of frequency response of WT grid side converter admittance when DC voltage control gains are 4 times higher

References

[1] C. Buchhagen, C. Rauscher, A. Menze, and J. Jung, "BorWin1 - First Experiences with harmonic interactions in converter dominated grids," in *International ETG Congress 2015*. Bonn: VDE,

2015, pp. 1–7.

[2] Working Group B4.55, "HVDC Connection of Offshore Wind Power Plants," CIGRE, Tech. Rep. May, 2015.

[3] Working Group B3.36, "Special Considerations for AC Collector Systems and Substations Associated with HVDC - Connected Wind Power Plants," CIGRE, Tech. Rep. March, 2015.

[4] A. Abdalrahman and E. Isabegovic, "DolWin1 - Challenges of connecting offshore wind farms," in *2016 IEEE International Energy Conference (ENERGYCON)*. IEEE, apr 2016, pp. 1–10.

[5] J. Sun, "Impedance-Based Stability Criterion for Grid-Connected Inverters," *IEEE Trans. Power Electron.*, vol. 26, no. 11, pp. 3075–3078, nov 2011.

[6] H. Saad, Y. Fillion, S. Deschanvres, Y. Vernay, and S. Dennetiere, "On Resonances and Harmonics in HVDC-MMC Station Connected to AC Grid," *IEEE Trans. Power Del.*, vol. 32, no. 3, pp. 1565–1573, jun 2017.

[7] M. Cheah-Mane, L. Sainz, J. Liang, N. Jenkins, and C. E. Ugalde Loo, "Criterion for the Electrical Resonance Stability of Offshore Wind Power Plants Connected through HVDC Links," *IEEE Trans. Power Syst.*, pp. 1–1, 2017.

[8] J. Lyu, M. Molinas, and X. Cai, "Stabilization control methods for enhancing the stability of wind farm integration via an MMC-based HVDC system," in *2017 11th IEEE Int. Conf. on Compatibility, Power Electronics and Power Engineering (CPE-POWERENG)*. IEEE, 2017, pp. 324–329.

[9] M. Amin and M. Molinas, "Understanding the Origin of Oscillatory Phenomena Observed Between Wind Farms and HVdc Systems," *IEEE J. Emerg. Sel. Topics Power Electron.*, vol. 5, no. 1, pp. 378–392, mar 2017.

[10] J. Lyu, X. Cai, and M. Molinas, "Frequency Domain Stability Analysis of MMC-Based HVdc for Wind Farm Integration," *IEEE J. Emerg. Sel. Topics Power Electron.*, vol. 4, no. 1, pp. 141–151, mar 2016.

[11] L. P. Kunjumuhammed, B. C. Pal, C. Oates, and K. J. Dyke, "Electrical Oscillations in Wind Farm Systems: Analysis and Insight Based on Detailed Modeling," *IEEE Trans. on Sustainable Energy*, vol. PP, no. 99, pp. 1–12, 2015.

[12] H. Liu and J. Sun, "Voltage Stability and Control of Offshore Wind Farms With AC Collection and HVDC Transmission," *IEEE J. Emerg. Sel. Topics Power Electron.*, vol. 2, no. 4, pp. 1181–1189, dec 2014.

[13] L. P. Kunjumuhammed, B. C. Pal, R. Gupta, and K. J. Dyke, "Stability Analysis of a PMSG-Based Large Offshore Wind Farm Connected to a VSC-HVDC," *IEEE Trans. on Energy Conversion*, vol. 32, no. 3, pp. 1166–1176, sep 2017.

[14] M. Cespedes and Jian Sun, "Mitigation of Inverter-Grid Harmonic Resonance by Narrow-Band Damping," *IEEE J. Emerg. Sel. Topics Power Electron.*, vol. 2, no. 4, pp. 1024–1031, dec 2014.

[15] S. Zhang, S. Jiang, X. Lu, B. Ge, and F. Z. Peng, "Resonance Issues and Damping Techniques for Grid-Connected Inverters With Long Transmission Cable," *IEEE Trans. Power Electron.*, vol. 29, no. 1, pp. 110–120, jan 2014.

[16] X. Wang, Y. W. Li, F. Blaabjerg, and P. C. Loh, "Virtual-Impedance-Based Control for Voltage-Source and Current-Source Converters," *IEEE Trans. on Power Electronics*, vol. 30, no. 12, pp. 7019–7037, dec 2015.

[17] L. Sainz, M. Cheah-Mane, L. Monjo, J. Liang, and O. Gomis-Bellmunt, "Positive-Net-Damping Stability Criterion in Grid-Connected VSC Systems," *IEEE J. Emerg. Sel. Topics Power Electron.*, pp. 1–1, 2017.

[18] L. Harnefors, "Modeling of Three-Phase Dynamic Systems Using Complex Transfer Functions and Transfer Matrices," *IEEE Trans. Ind. Electron.*, vol. 54, no. 4, pp. 2239–2248, aug 2007.

[19] L. Harnefors, X. Wang, A. G. Yepes, and F. Blaabjerg, "Passivity-Based Stability Assessment of Grid-Connected VSCsAn Overview," *IEEE J. Emerg. Sel. Topics Power Electron.*, vol. 4, no. 1, pp. 116–125, mar 2016.

[20] J. Sun and H. Liu, "Sequence Impedance Modeling of Modular Multilevel Converters," *IEEE Journal of Emerging and Selected Topics in Power Electronics*, vol. 5, no. 4, pp. 1427–1443, 2017.

[21] X. Wang, F. Blaabjerg, and W. Wu, "Modeling and Analysis of Harmonic Stability in an AC Power-Electronics-Based Power System," *IEEE Trans. Power Electron.*, vol. 29, no. 12, pp. 6421–6432, dec 2014.

[22] L. Harnefors, A. G. Yepes, A. Vidal, and J. Doval-Gandoy, "Passivity-Based Controller Design of Grid-Connected VSCs for Prevention of Electrical Resonance Instability," *IEEE Trans. Ind. Electron.*, vol. 62, no. 2, pp. 702–710, feb 2015.

[23] M. Cespedes and J. Sun, "Modeling and mitigation of harmonic resonance between wind turbines and the grid," in *2011 IEEE Energy Conversion Congress and Exposition*. IEEE, sep 2011, pp. 2109–2116.

[24] L. Harnefors, M. Bongiorno, and S. Lundberg, "Input-Admittance Calculation and Shaping for Controlled Voltage-Source Converters," *IEEE Trans. Ind. Electron.*, vol. 54, no. 6, pp. 3323–3334, dec 2007.

[25] L. Harnefors, R. Finger, X. Wang, H. Bai, and F. Blaabjerg, "VSC Input-Admittance Modeling and Analysis Above the Nyquist Frequency for Passivity-Based Stability Assessment," *IEEE Transactions on Industrial Electronics*, vol. 64, no. 8, pp. 6362–6370, aug 2017.